

Extended Ly α emission from a damped Ly α absorber at $z = 1.93$, and the relation between DLAs and Lyman-break galaxies

J. U. Fynbo^{1,2,3}, P. Møller^{1,3,4} and S. J. Warren⁵

¹*European Southern Observatory, Karl-Schwarzschild-Straße 2, D-85748 Garching, Germany*

²*Institute of Physics and Astronomy, University of Århus, DK-8000 Århus C, Denmark*

³*Space Telescope Science Institute, 3700 San Martin Drive, Baltimore, MD21218, USA*

⁴*on assignment from the Space Science Department of ESA*

⁵*Blackett Laboratory, Imperial College of Science Technology and Medicine, Prince Consort Rd, London SW7 2BZ, UK*

Accepted 1998 ???. Received ???; in original form ???

ABSTRACT

The number of damped Ly α absorbers (DLAs) currently known is about 100, but our knowledge of their sizes and morphologies is still very sparse as very few have been detected in emission. Here we present narrow-band and broad-band observations of a DLA in the field of the quasar pair Q0151+048A (qA) and Q0151+048B (qB). These two quasars have very similar redshifts $z_{em}=1.922, 1.937$, respectively, and an angular separation of 3.27 arcsec. The spectrum of qA contains a DLA at $z_{abs} = 1.9342$ (close to the emission redshift) which shows an emission line in the trough, detected at 4σ . Our narrow-band image confirms this detection and we find Ly α emission from an extended area covering 6×3 arcsec², corresponding to $25 \times 12 h^{-2}$ kpc² ($q_0=0.5, H_0 = 100 h$ km s⁻¹). The total Ly α luminosity from the DLA is 1.2×10^{43} h⁻² erg s⁻¹, which is a factor of several higher than the Ly α luminosity found from other DLAs. The narrow-band image also indicates that qB is not covered by the DLA. This fact, together with the large equivalent width of the emission line from the Ly α cloud, the large luminosity, and the ~ 300 km s⁻¹ blueshift relative to the DLA, can plausibly be explained if qB is the source of ionising photons, lying to the near side of the DLA at a distance from the DLA of $< 20 h^{-1}$ kpc. In this case the size of the emission-line region corresponds to the area over which the cloud is optically thick, i.e. is indicative of the size of a Lyman-limit system. We also consider the relation between DLAs and Lyman-break galaxies (LBGs). If DLAs are gaseous disks surrounding LBGs, and if the apparent brightnesses and impact parameters of the few identified DLAs are representative of the brighter members of the population, then the luminosity distribution of DLAs is nearly flat, and we would expect that some 70% of the galaxy counterparts to DLAs at $z \approx 3$ are fainter than $m_R = 28$.

Key words: galaxies : formation – quasars : absorption lines – quasars : individual : Q0151+048.

1 INTRODUCTION

The quest for non-active galaxies at high redshift has gone through a dramatic change in the last few years. The number of galaxies at $z > 2$ found using the Lyman-break technique (Steidel et al., 1996) is now counted in hundreds, providing information on the global density of star formation at early epochs, and the evolution of galaxy clustering. A different perspective on the formation of galaxies is obtained by studying the population of damped Ly α absorbers (DLAs), the objects responsible for the strongest absorption lines seen in the spectra of quasars. The advantage of DLAs is

that they provide a wealth of information on the chemical evolution of galaxies in the form of the measurement of the metallicity and dust content of the gas (e.g. Lu et al., 1996, Pettini et al., 1997, Kulkarni and Fall, 1997). The DLAs have column densities larger than 2×10^{20} cm⁻², comparable to the column density for a sightline through the disk of a nearby spiral galaxy. In addition the total gas content in DLAs is similar to the mass in stars and gas at the present epoch (Wolfe et al., 1995). For these reasons DLAs are widely believed to be the gas reservoirs from which today's spiral galaxies formed.

The relation between DLAs and Lyman-break galaxies (LBGs) is unclear at present because very few DLAs have been unambiguously detected in emission. At low and intermediate redshifts $z < 1$ a number of candidate counterparts of DLAs have been discovered in deep images (Steidel et al. 1994, 1995, LeBrun et al. 1997). These candidates display a mix of morphological types from spiral galaxies to very compact objects (LeBrun et al. 1997), but so far none has spectroscopic confirmation. At high redshift there are three DLAs which have been imaged and for which confirmatory spectroscopy exists; the DLA at $z_{abs}=2.81$ towards PKS0528–250 (Møller & Warren, 1993b), the DLA at $z_{abs} = 3.150$ towards Q2233+131* (Djorgovski et al., 1996), and the DLA at $z_{abs} = 4.10$ towards DMS2247-0209 (Djorgovski, 1998). The first of these has been imaged with HST (Møller & Warren, 1998) and has a continuum half light radius of 0.13 ± 0.06 arcsec, similar to that measured for the LBGs (Giavalisco et al., 1996).

Information on the gas sizes of DLAs comes from the measured impact parameters. Combined with the line density of absorbers dn/dz the space density may be computed. Møller & Warren, 1998 produced a preliminary estimate of the space density of high-redshift DLAs by using the impact parameters of confirmed and candidate counterparts. The data suggest that for $q_0 = 0.5$ the space density of DLA clouds at $z > 2$ is more than five times the space density of spiral galaxies locally. For $q_0 = 0.0$ there is no evidence as yet that DLA clouds are more common than spiral galaxies locally. A single measurement of 21cm absorption against an extended radio source, the quasar 0458-020, by Briggs et al. (1989), provides additional information on the size of DLAs. Their analysis indicates that the DLA seen in the spectrum of this quasar has a gas size greater than $8h^{-1}$ kpc.

It would clearly be useful to image more high-redshift DLAs, to understand better their relation to LBGs, but also to measure the star formation rates and connect these to the rate of consumption of gas (Pei and Fall 1995). In this paper we present observations of a DLA in the field of the quasar pair Q0151+048A (qA) and Q0151+048B (qB). The two quasars have very similar redshifts $z_{em}=1.922$ and 1.937 respectively (Møller, Warren & Fynbo 1998), and an angular separation of 3.27 ± 0.01 arcsec. The spectrum of qA contains a DLA at $z_{abs} = 1.9342$, close to the emission redshift, and this was the reason we originally chose this system for study because of the possibility of detecting Ly α emission due to photoionisation by either of the quasars (see Møller & Warren (1993a,b) for a detailed discussion of the predicted effect). In Møller, Warren & Fynbo 1998, we presented a spectrum of qA which shows an emission line in the DLA trough, detected at 4σ . The present paper describes follow-up narrow-band and broad-band imaging observations of this system.

In section 2 we describe the observations and the data reduction. In section 3 we describe the PSF-subtraction of qA and qB and the photometry of the objects found in the field. In section 4 we discuss the results obtained. Through-

* When comparing DLA emitters to statistical samples of DLA absorbers, it is important to remember that this object does not meet the N(HI) criterion of a DLA absorber. Statistically speaking this is a Lyman-Limit System

Table 1. Observations of Q0151+048A,B, 1996 Sept 15 – 18

Filter	Combined seeing	Exposure sec
CS 3565/20	1.1	62700
U	0.9	12000
I	0.8	7800

out this paper we adopt $q_0 = 0.5$, $H_0 = 100h$ km s $^{-1}$ Mpc $^{-1}$ and $\Lambda = 0$ unless otherwise stated.

2 OBSERVATIONS AND DATA REDUCTION

The data were obtained with the 2.56-m Nordic Optical Telescope (NOT) during four nights beginning September 15, 1996. Observations of the Q0151+048A,B field were done in three bands: the standard U and I filters, and a special narrow-band filter manufactured by Custom Scientific. The narrow-band filter (CS 3565/20) is tuned to Ly α at the redshift of the DLA $z = 1.9342$. It has a central wavelength of $\lambda_{3565\text{\AA}}$ and a full width at half maximum (FWHM) of 20\AA . The peak transmission of the filter is $T(\lambda)_{max} = 0.385$ and red leak is less than 10^{-6} to 1.2μ . The CCD used was a 1024^2 back-side illuminated thinned Tektronix with a pixel scale of 0.1757 ± 0.002 arcsec and read noise of $5.4e^-$. The QE in the near UV for this detector rises from 0.3 at 3500\AA to 0.6 at 4000\AA .

Conditions were photometric during most of the run allowing accurate calibration data to be obtained. The seeing ranged from 0.80 arcsec to 1.35 arcsec FWHM in the narrow-band frames and from 0.60 arcsec to 1.30 arcsec FWHM in the U and I frames. Integration times were in most cases 4000 seconds for the narrow-band frames, 1000 seconds for the U, and 300 seconds for the I, ensuring that the noise in each frame is dominated by photon noise from the sky and not by read noise. Between exposures the telescope pointing was jittered in steps of 2 to 5 arcsec to minimize the effect of bad pixels. The total integration times in the different filters are listed in Table 1, together with the measured seeing in the combined frames. For the calibration we observed Landolt (1992) photometric standards for the broad-band data, and the HST spectrophotometric standards GD71, BD284211 and BD254655 (Colina and Bohlin, 1994) for the narrow-band data.

Bias and dark frames were firstly subtracted from the data frames. Twilight sky frames were obtained and were used to flatten the U and I data directly. For the narrow-band frames however we found that the instrument setup allowed a small, but significant, amount of light to reach the CCD without passing through the filter. This additional source of background light, which could be either light scattered around the filter wheel or light leaking through the camera enclosure, was too weak to be detectable in the broad-band images, but was a very significant contribution in the narrow-band images. Here we shall refer to this source as scattered light.

The scattered light produced a pattern mostly across the upper two thirds of the CCD. We applied a correction

for this as follows. Firstly the contribution to the twilight sky frames was measured by placing a blocking filter in the filter wheel. From these frames we determined a model of the scattered light by median and Gaussian filtering. This model was then scaled and subtracted from the flat frames prior to the creation of the normalised master-flat. The scattered light in the data frames did not have exactly the same structure across the CCD as in the flat-field frames. The reason for this is not known, but it is possibly due to a different position of the guide probe. We therefore modelled the scattered light in the data frames by summing all the frames, having removed all objects by interpolation and filtering. This model was then scaled to, and subtracted from, the individual data frames. After flat fielding the residual large scale variations left were less than 5%.

The frames for each filter were then divided in two groups depending on whether the seeing was greater or smaller than 1 arcsec FWHM, in order to optimize the combination of the frames. Both groups were then registered by integer pixel shifts to a common coordinate system and the frames within each group were combined using the optimal combination code described by Møller & Warren (1993b), which maximizes the signal-to-noise ratio for faint sources. The model for the scattered light was included in the calculation of photon noise from the sky. Finally, the two summed frames for each filter were combined by weighting by the inverse of the sky variance.

All magnitudes quoted in this paper are on the AB system. The narrow-band data were calibrated directly onto the AB system, and magnitudes are denoted $n(AB)$. For the U band we determined the colour equation $u = U + 0.26(U - B)$ relating the instrumental magnitude u to the standard Johnson U . The fit to the U colour equation used data for seven different stars but is not well determined. There was substantial scatter about the fit near $U - B = 0$, ~ 0.05 mag., and evidence that the relation is non-linear. Such results are typical for this band (e.g. Bessell 1990). The instrumental magnitudes u were converted to AB magnitudes using the equation $u(AB) = u + 0.49$, determined by integrating the spectrum of the star GD71 over the passband. Here we have retained the lower case u for the AB magnitude indicating that the effective wavelength of the filter lies significantly away from the standard value. The colour term for the I filter is consistent with zero i.e. $i = I$, and we used the equation $I(AB) = I + 0.43$ (Fukugita et al 1995) to put the magnitudes onto the AB system. Details of the sky noise in the combined images are provided in Table 2.

3 RESULTS

The field of the quasar pair is illustrated in Fig. 1 which shows the final combined I (upper) and narrow-band (lower) images. The quasars Q0151+048A,B lie near the centre and are marked qA and qB. Also marked on the image are two bright stars (psfA and psfB) and a source, named S5, to be discussed later (Section 3.3).

See attached GIF colour image.

Figure 1. Field containing the quasar pair Q0151+048A,B. *Upper:* combined I frame, *Lower:* combined narrow-band frame. The field shown is 920x920 pixels, 162x162 arcsec². North is up and east to the left. The two quasars are marked qA and qB. The two bright stars marked psfA and psfB were used for determination of the point spread function. The galaxy marked S5 is discussed in the text (Section 3.3).

Table 2. Measured rms of sky surface brightness. For the narrow-band we provide a range due to the presence of the scattered light gradient across the field.

passband	rms SB
	mag. arcsec ⁻²
I(AB)	26.9
u(AB)	25.6
n(AB)	25.7-25.8

3.1 Ly α emission near Q0151 + 048

In the narrow-band image faint emission is seen extending to the east of qA. To get a clearer view of this in Fig. 2a (upper panel) we show a contour plot of a small section from the centre of the narrow-band image. Here, in addition to the images of the two quasars, a plume of emission, presumably Ly α from the DLA, is clearly seen extending towards the east of qA. To reveal the full extent of the Ly α emission we subtracted the images of the two quasars as follows.

The two bright stars marked psfA and psfB in Fig. 1 were used with DAOPHOT II (Stetson, 1994) to define the point-spread function (PSF). The complex image made up of the extended Ly α emitter super-imposed on the images of the two quasars was decomposed by iteration. First DAOPHOT II was used to fit, and subtract, the two point sources. Because of the Ly α emission this will oversubtract the point sources. We then used a galaxy model to

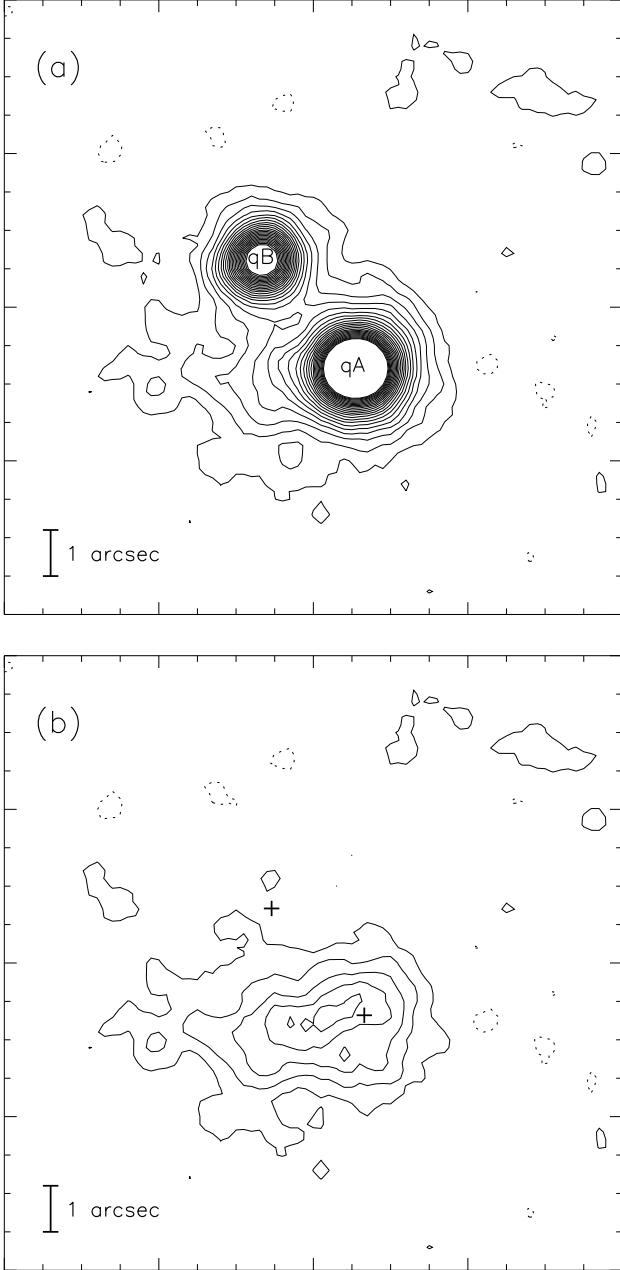


Figure 2. Contour plot of the narrow-band frame showing the 80x80 pixels region, 14x14 arcsec², surrounding the two quasars. North is up and east to the left. The frame has been smoothed by convolution with a Gaussian with σ corresponding to the PSF. *Upper:* final combined frame showing the two quasars marked qA and qB and excess emission east of qA. The contour levels are at -3, 3, 6, 9, ... $\times 10^{-17}$ erg s⁻¹ cm⁻² arcsec⁻², with the dotted contours being negative. *Lower:* final combined frame (same contour levels as above) after subtraction of the quasar images, revealing Ly α emission from the object S4 over a region 6x3 arcsec². The positions where quasar psfs were subtracted are marked by crosses.

fit the residuals finding the minimum- χ^2 fit of the model convolved with the psf (as in e.g. Warren et al. 1996). The model consists of an exponential surface-brightness profile $\Sigma = \Sigma_s \exp(-r/r_s)$, and elliptical shape with constant ellipticity and orientation. Here r is equal to \sqrt{ab} i.e. the geometric mean of the semi-major and semi-minor axes. We tried a range of surface-brightness profiles but the exponential function provided the best fit. The best-fit galaxy model was then subtracted from the original image, and a second iteration of DAOPHOT II fitting to the quasar images followed. After 9 rounds of alternating point source subtraction and exponential-disc fitting the procedure reached a stable solution. The frame after subtraction of the images of the two quasars is shown in Fig. 2b. The parameters of the fit are $r_s = 0.95$ arcsec, a central surface brightness of 3.3×10^{-16} erg s⁻¹ cm⁻² arcsec⁻², ellipticity $e = 0.53$, and PA 98° (E of N). The probability associated with the χ^2 of the final fit to the Ly α emission is 4%. This rather small value is explained by the asymmetric light profile which falls off more sharply to the W than to the E.

In Fig. 2b emission is seen from an elongated structure of dimensions approximately 6 x 3 arcsec². In the following we shall refer to this source of Ly α emission as S4. To perform photometry of objects in the field we used the package SExtractor (Bertin & Arnouts, 1996) and determined *isophotal* magnitudes and so called *Automatic Aperture* magnitudes (AAMs), as described below. The magnitudes of the three objects S4, qA, and qB, were measured individually in frames from which the images of the other two objects had been subtracted. The magnitudes of other objects in the vicinity were measured in frames from which all three images had been removed.

With the exception of S4 the apertures for the *isophotal* magnitudes were set by reference to the frame formed by summing the combined frames for the three passbands. This frame was convolved with a Gaussian detection filter with FWHM equal to the seeing. The isophotes set at 1.5 times the noise measured in the unconvolved frame defined the apertures and the same apertures were then applied to each passband. The detection limit for faint objects was set at a minimum aperture size of 5 pixels (total). Hence, the *isophotal* magnitudes provide photometry appropriate for accurate colour determination. For S4 the same procedure was followed, but only the narrow-band frame was used. Finally, since the catalogue is defined by detection in the three-passband combination frame, we also ran SExtractor on the narrow-band frame and found that, with the exception of S4, no source detected in the narrow-band frame at $S/N > 4$ had been overlooked.

The AAM is intended to give the best estimate of the total flux and is measured using an elliptical aperture with minor axis $b = 2.5r_1\epsilon$ and major axis $a = 2.5\frac{r_1}{\epsilon}$, where r_1 is the first moment of the light distribution and ϵ is the ellipticity. The isophotal narrow-band magnitude and the AAM for S4 correspond to fluxes of $9.0 \pm 0.4 \times 10^{-16}$ and $1.91 \pm 0.07 \times 10^{-15}$ erg s⁻¹ cm⁻² respectively. The AAM for S4 ($n(\text{AB})=19.95 \pm 0.04$) agrees well with the total magnitude of the fitted galaxy model ($n(\text{AB})=20.01$).

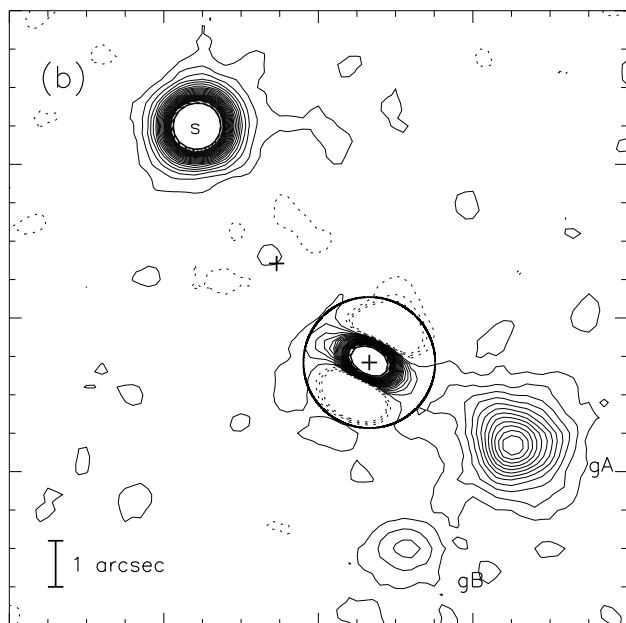
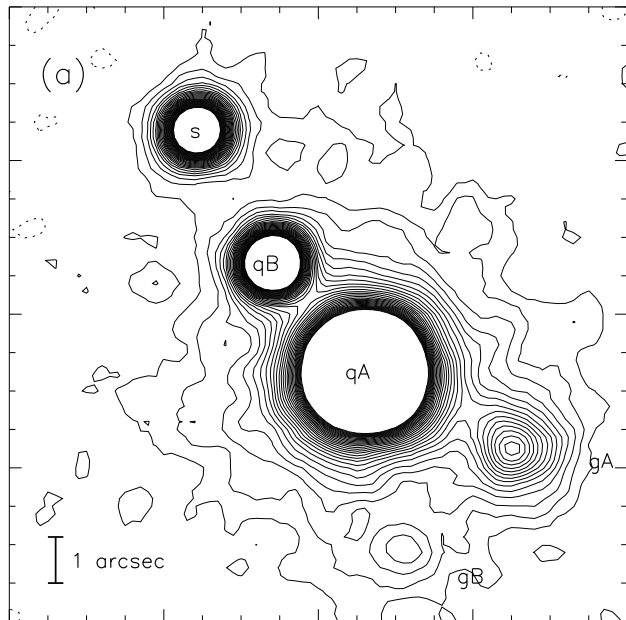


Figure 3. I-band contour plot of the same field as in Fig. 2. *Upper:* final combined frame showing, in addition to the two quasars, two faint galaxies marked gA and gB, and a star marked s. The contour levels are $-9, -6, -3, 3, 6, \dots \times 1\sigma$ of the sky noise, with the dotted contours being negative. *Lower:* final combined frame (same contour levels as above) after subtraction of the quasar images.

3.2 Broad-band photometry of S4

Fig. 3a shows a contour plot of the I band image of the same field as in Fig. 2. Here we see the two quasars, a star north-east of the quasars which was not visible in the narrow band image, and two faint galaxies marked gA and gB south-west of the quasar qA. In Fig. 3b psfs have been subtracted at the positions of the two quasars, leaving behind only the star and the two faint galaxies. In Fig. 3b we have also overlaid

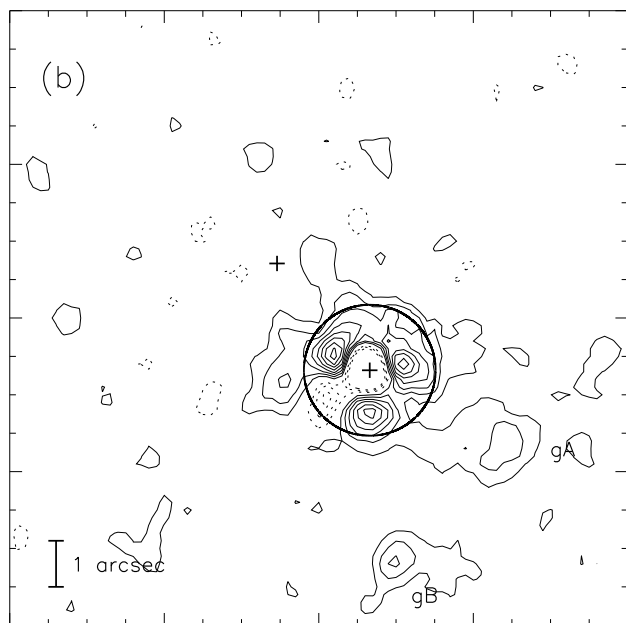
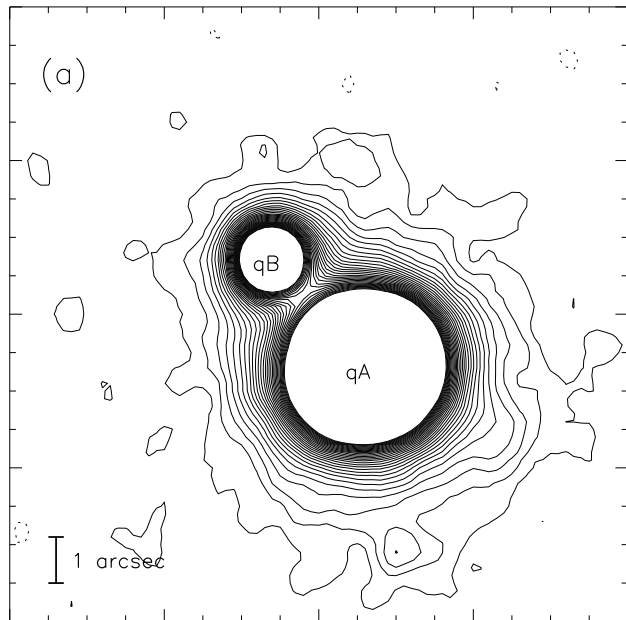


Figure 4. U-band contour plot of the same field as in Fig. 2. *Upper:* final combined frame showing the two quasars. The contour levels are $-9, -6, -3, 3, 6, \dots \times 1\sigma$ of the sky noise, with the dotted contours being negative. *Lower:* final combined frame (same contour levels as above) after subtraction of the quasar images.

a circle of radius 1.5 arcsec centred on the position of qA. The strong residuals from the psf-subtraction prevent any detection of additional faint sources within this region.

In Fig. 4a we show the U-band contour plot of the same region, and in Fig. 4b again the field after subtraction of the quasar images. Also in Fig. 4b we have overlaid a circle of radius 1.5 arcsec centred on the position of qA. In the psf-subtracted U image we see the two faint galaxies gA and gB, but in addition there is a faint extension about 2 arcsec east of qA, roughly at the position of S4.

Table 3. Photometric properties of the quasars qA and qB, of the faint galaxies S4, S5, gA and gB, and of the star s. Magnitudes of extended objects have been determined in two apertures (isophotal and AAM, both defined in Sect. 3.1). For the point sources we only provide AAM. Note that magnitudes marked ^a are not true AAM magnitudes, they were determined via scaling of the fitted exponential-disk model as detailed in Sect. 3.2. Lower limits to magnitudes (upper limits to fluxes) are 2σ . For gA and gB the determination of reliable apertures for AAM was impossible due to the nearness of strong residuals of the QSO PSF-subtraction.

Object	u(AB)	I(AB)	n(AB)	Apert. (pix)
Isoph.				
S4			20.76 ± 0.05	254
S5	24.60 ± 0.10	24.04 ± 0.09	24.1 ± 0.2	37
gA	24.28 ± 0.12	22.00 ± 0.04	> 24.0	170
gB	26.0 ± 0.2	24.88 ± 0.14	> 25.3	18
AAM				
qA	17.90 ± 0.02	17.49 ± 0.02	19.72 ± 0.04	241
qB	21.07 ± 0.03	20.87 ± 0.02	20.04 ± 0.03	241
s	> 25.6	20.98 ± 0.02	> 23.8	341
S4	$22.9^a \pm 0.2$	$22.8^a \pm 0.3$	19.95 ± 0.04	690
S5	24.01 ± 0.09	23.70 ± 0.11	23.6 ± 0.2	241

The narrow band image shows that S4 is extended and that it covers the bright quasar qA. Therefore, when observed through a broad band filter the tail of the psf of qA extends across most of S4 and will, even under good seeing conditions, make the determination of broad-band magnitudes of S4 an extremely difficult task. Simple aperture photometry, after fitting and subtracting the quasar psf, is not possible because of the strong residuals from the psf-subtraction, and because there is a degeneracy in the determination of how much of the faint extended flux is due to the tail of the quasar psf, and how much is due to S4. In order to break this degeneracy, and to obtain an objective measure for the broad-band magnitudes of S4 we proceeded as follows:

On the assumption that the broad-band flux can be fitted by the exponential-disk model defined by the fit to the narrow-band flux, we firstly subtracted a scaled narrow-band model from the broad band image. We then subtracted a psf at the position of qA. The quasar psf was scaled so that the integrated residual flux measured in a rectangular aperture (5.6 arcsec by 3.3 arcsec) covering both the quasar and the central region of S4, was exactly zero. This calculation was performed for a range of values of the scaling of the model for S4, and for each combination of S4-model and quasar psf the total χ^2 of the fit to the data was calculated. The I and U band magnitudes of S4 provided in Table 3 are those corresponding to the quasar-psf/S4-model combinations providing the minimum χ^2 . The errors quoted are those where χ^2 increased by one. The rectangular aperture was defined so as not to include flux from the galaxy gA. The χ^2 was calculated in a smaller aperture to exclude the central part of the quasar psf where it would be dominated by noise from the strong central psf-residuals. Table 3 pro-

vides a summary of the photometry of the object S4, both quasars, and several other objects found in the field.

Møller & Warren, 1998 found evidence that a DLA-galaxy at $z=2.81$, as well as its two companion galaxies, all had one (or more) compact cores of continuum-emission, while the Ly α emission from the same objects extended over larger areas. If this is a general feature of high redshift galaxies we could expect to see one (or several) continuum emitting cores in S4. Our current data are not adequate to resolve this question. Clearly higher resolution and deeper broad-band imaging is required.

3.3 The impact parameter b_{DLA} of S4

In Møller & Warren (1998) the DLA impact parameter b_{DLA} was defined as the projected distance between the line-of-sight to the quasar to that of the centroid of the continuum flux of the DLA absorber. In the case of Q0151+048 we clearly see extended Ly α emission from the DLA absorber, and our analysis of the broad band data shows that they are not inconsistent with a broad-band flux distribution identical to that of the Ly α flux. The centroid of the model fit to the narrow-band data is located 0.93 arcsec east, 0.03 arcsec south of Q0151+048A ($b_{\text{DLA,Ly}\alpha} = 0.93$ arcsec), and we shall for now adopt this as the impact parameter of the DLA in Q0151+048A.

3.4 Ly α in the surrounding field

An object with Ly α emission at $z=1.93$ will appear bright in the narrow-band compared to U and I, so we can use the results of the photometry to search for other Ly α emitters in the field. In Fig. 5 we plot the $n(AB) - u(AB)$ versus $n(AB) - I(AB)$ two-colour diagram for all objects detected at a signal-to-noise ratio larger than 4 in the narrow-band frame. Strong Ly α emitters at $z = 1.93$ will lie in the lower left region of this diagram. Conversely an object with absorption in the narrow-band filter will lie in the upper right corner. Since our narrow-band filter is fairly well centred in the U-band most objects will have zero $n(AB) - u(AB)$ colour, and horizontal lines in Fig. 5 are to a good approximation lines of constant equivalent absorption or emission line width. Lines of constant continuum $U - I$ will appear as diagonals in Fig. 5 with the bluest objects in the upper left corner and red objects in the lower right. The dashed curve shows the location of a series of simulated objects with identical power-law continuum on which is superimposed absorption or emission lines of different strengths in the narrow pass-band. The curve mostly falls along a diagonal of the constant $U - I$ of the continuum, but bends to the left as the emission line starts to dominate the flux in the U-band filter. The dashed curve approaches asymptotically a model with an emission line of infinite equivalent width (dot-dash line).

The quasar qA lies in the upper part of the diagram, as expected because of absorption by the DLA. Conversely the quasar qB lies in the lower left part of the diagram. The filter is too narrow to contain all of the Ly α emission line for the quasar qB, but even so the $n(AB) - u(AB)$ implies that the mean flux level over the narrow-band filter is at a level three times greater than the average over the U band.

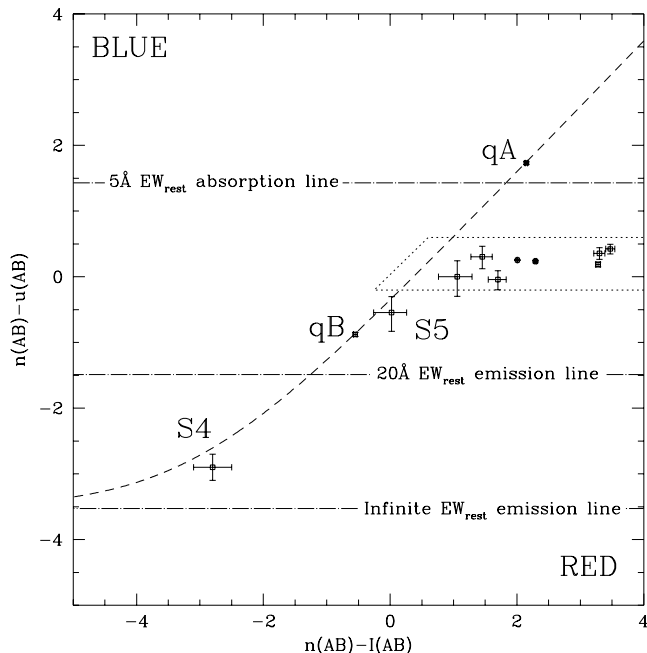


Figure 5. Two-colour diagram $n(AB) - u(AB)$ versus $n(AB) - I(AB)$ for the 11 detected objects with signal-to-noise ratio in the narrow-band frame > 4 . The dashed line is a line of constant $u - I$ in the continuum indicating that the two quasars have very similar $u - I$ continuum colours but very different Ly α line equivalent widths (EWs). The dotted lines confine the expected region of objects with no special features in the narrow filter. The horizontal lines are lines of constant rest-frame $EW=20\text{\AA}$ for an emission line at $z = 1.93$ (lower) and rest-frame $EW=5\text{\AA}$ for an absorption line (upper) that lies in the narrow-band filter.

Therefore the DLA seen in the spectrum of the quasar qA cannot be present in the spectrum of qB. If the quasar qB also lies behind the cloud responsible for the DLA, then the column density is much lower at the position of qB.

There is another candidate Ly α emitter seen in Fig. 5, marked S5. The location of this candidate is shown in Fig. 1. The object is detected at a S/N of 4.8, 14, and 13 in the narrow, U, and I band images respectively. The corresponding flux of the candidate Ly α line is $6.6 \pm 1.3 \times 10^{-17}$ erg cm $^{-2}$ s $^{-1}$ and the restframe equivalent width of the line is $9\text{\AA} \pm 2\text{\AA}$. The angular separation of S5 from the line of sight to the quasar is 40.9 arcsec, which corresponds to 169 h $^{-1}$ kpc ($q_0=0.5$) and 263 h $^{-1}$ kpc ($q_0=0.0$) at $z = 1.93$.

4 DISCUSSION

4.1 The origin of the large Ly α luminosity

The Ly α luminosity of S4 is 1.2×10^{43} h $^{-2}$ erg s $^{-1}$. Other high redshift DLAs for which the Ly α flux has been measured are the DLA at $z = 2.81$ towards PKS0528–250 (Møller & Warren, 1993b), the DLA at $z_{abs} = 3.150$ towards Q2233+131 (Djorgovski et al., 1996), and the DLA at $z_{abs} = 3.083$ towards Q2059–360 (Pettini et al 1995, Robertson and Leibundgut 1997, Leibundgut and Robertson 1998). The last

is a spectroscopic detection of spatially resolved excess emission in the DLA absorption trough. The Ly α luminosities for these DLAs are collected in Table 4 and we have assumed a flux of 2×10^{-16} erg s $^{-1}$ cm $^{-2}$ for Q2059–360 based on details in Leibundgut and Robertson (1998). The measured luminosity for Q0151+048 stands out, being several times larger than the other values. In this section we consider possible explanations for this anomaly.

In the light of the dearth of successful detections of emission from DLAs it is noticeable that of the four high-redshift DLAs listed in Table 4, three have redshifts close to the quasar emission redshift. This point was noted by Møller et al (1998) who suggested that photoionisation by the quasar was a plausible explanation for the Ly α emission for Q0151+048 and Q2059–360, although not for PKS0528–250 where the continuum emission detected from the DLA is sufficient to account for the Ly α emission (Møller & Warren, 1998), and where recent spectroscopic observations (Ge et al., 1997) has ruled out that the quasar could be the source of the ionisation. In the case of Q0151+048 there are two quasars potentially close to the DLA galaxy. Q0151+048B is not only close to the line of sight to the DLA galaxy, it also has a redshift (1.937 ± 0.005 , Møller et al 1998) consistent with being identical to that of the DLA galaxy. For this reason, one may slightly favour qB as the source of ionisation. Q0151+048A, on the other hand, has a redshift which (if interpreted as due to peculiar motion) indicates that it is moving towards qB and the DLA galaxy with a velocity of about 1200 km s $^{-1}$. We now consider the possibility of photoionisation for the Q0151+048 DLA galaxy in more detail.

The relative distances of qA, qB, and the DLA cannot be determined from the redshifts because of peculiar velocities. The DLA lies in front of qA, since it absorbs it, but qB could lie either at larger or smaller distance than the DLA. If qB is beyond the DLA then the region of high-column density of the absorber does not extend across it. This is because the $n(AB) - u(AB)$ colour of qB corresponds to an average flux level in the n band of three times the continuum level (Fig 5), so the Ly α emission line of qB is not strongly absorbed. One possible explanation for the extended Ly α emission is that qB lies nearer than the DLA and lights up the near face of the absorber (Fynbo, Møller, and Warren, 1998). However it is also possible that qA is the source of photoionisation. Since qA under this assumption illuminates the backside of the absorber, in the simplest picture one would expect to see a hole in the Ly α emission, containing the line of sight to the quasar, over the area where the optical depth is high since over this region the Ly α photons escape out of the back of the absorber. Ly α photons would only be detectable from an annulus around the DLA where the optical depth is approximately unity. However if DLA clouds are sufficiently inhomogeneous on scales much smaller in extent than the seeing disk, the hole may not be seen as Ly α photons could travel between the densest regions.

The velocity offset of the emission line relative to the DLA for Q0151+048 provides an additional clue to the spatial arrangement of the three objects qA, qB, and S4. The emission line detected for S4 is offset by ~ 300 km s $^{-1}$ to the blue of the DLA redshift (Møller et al 1998). In the case of Q2059–360 the emission line lies 490 km s $^{-1}$ to the red of the DLA redshift (Leibundgut and Robertson 1998). One

Table 4. Measured Ly α luminosities in high-redshift DLAs

quasar	z_{em}	z_{abs}	luminosity	reference
Q0151+048	1.92	1.93	$1.2 \times 10^{43} \text{ h}^{-2}$	this paper
PKS0528–250	2.79	2.81	$1.1 \times 10^{42} \text{ h}^{-2}$	Møller & Warren (1993b)
Q2059–360	3.10	3.08	$3.7 \times 10^{42} \text{ h}^{-2}$	Pettini et al (1995), Leibundgut and Robertson (1998)
Q2233+131	3.30	3.15	$1.2 \times 10^{42} \text{ h}^{-2}$	Djorgovski et al. (1996)

possible explanation of those velocity differences is that they are a consequence of photoionisation by the quasar. The radiation pressure of the resonantly scattered Ly α photons would cause the HII skin of the DLA to expand away from the HI in the direction of the quasar (Williams 1972, Urbaniak and Wolfe 1981). This would provide an explanation of why the emission line for Q2059–360 is redshifted relative to the DLA. In this case some of the Ly α photons, produced on the far side, are able to penetrate the cloud because of the reduced optical depth in the red wing of the damped absorption line. Those photons would be observed as a redshifted emission line. For Q0151+048 the blueshift of the emission line would imply that qB is the source of ionising photons and must lie on the near side of the DLA.

The above arguments are far from conclusive, but the picture that qB is the source of ionising photons is at least plausible. We can make this statement more quantitative by computing how near qB must lie in order to explain the flux observed. To do this we follow the analysis presented by Warren and Møller (1996, their equations nos 1 and 2). Consider a disk of HI of large optical depth, at distance d from a quasar of absolute magnitude M_B , and with normal inclined at angle ϕ to the line from the quasar to the cloud. The surface brightness of the cloud over the region of high optical depth is given by:

$$\Sigma_{Ly\alpha} = 3.66 \times 10^{-22} \frac{10^{-0.4M_B}}{d^2} \frac{\cos\phi}{\alpha} \left(\frac{912}{4400}\right)^\alpha \text{ erg s}^{-1} \text{ cm}^{-2} \text{ arcsec}^{-2}$$

where α is the quasar continuum slope in the power-law representation $f_\nu \propto \nu^{-\alpha}$, and d is in kpc. Therefore the distance of the quasar is given by

$$d = \sqrt{3.66 \times 10^{-22} \frac{10^{-0.4M_B}}{\Sigma_{Ly\alpha}} \frac{\cos\phi}{\alpha} \left(\frac{912}{4400}\right)^\alpha} \text{ kpc}$$

We set $\Sigma_{Ly\alpha}$ equal to the peak surface brightness for the model fit to S4 (§3) $\Sigma_{Ly\alpha} = 3.3 \times 10^{-16} \text{ erg s}^{-1} \text{ cm}^{-2} \text{ arcsec}^{-2}$ i.e. where the surface brightness peaks the optical depth of HI visible to the quasar is assumed to be very high, and the drop off in surface brightness from the peak corresponds to a decline in column density. The absolute magnitude for the quasar is computed from the apparent magnitude $I(AB) = 20.87$, Table 3. The upper limit to the distance of qB from the cloud is then obtained by setting $\cos\phi = 1.0$. For values of $\alpha = 0.7$ and 1.0 we find $d < 20 \text{ h}^{-1}$ kpc and $< 14 \text{ h}^{-1}$ kpc, respectively, for $q_0 = 0.5$. For $q_0 = 0.0$ the values are $d < 32 \text{ h}^{-1}$ kpc and $< 23 \text{ h}^{-1}$ kpc. These values are all the more plausible since they are larger than, but similar to, the projected distance from qB to the DLA, 12 h^{-1} and 19 h^{-1} , for $q_0 = 0.5$ and $q_0 = 0.0$ respectively. This

means that the Ly α emission can be explained by photoionisation by qB without having to invoke an unlikely geometry. For example for $q_0 = 0.5$, setting $\cos\phi = 0.7$, $\alpha = 1.0$, leads to $d = 14.5 \text{ h}^{-1}$ kpc, which corresponds to an angle $\theta = 30^\circ$ between the line joining qB to the DLA and the plane of the sky. The boundary of detectable Ly α emission corresponds to the point where the optical depth in HI becomes small. In other words the quasar is highlighting a Lyman-limit system. The size of the DLA contained would be smaller.

For completeness we consider the possibility that the photoionisation model is not correct and that the Ly α emission is due to star formation. Using the Kennicutt (1983) prescription $\text{SFR} = L(\text{H}\alpha)/1.12 \times 10^{41} \text{ erg s}^{-1}$ and assuming $L(\text{Ly}\alpha)/L(\text{H}\alpha)=10$ and negligible dust extinction leads to

$$\text{SFR} = 11(26) \text{ h}^{-2} M_\odot \text{ yr}^{-1} q_0 = 0.5(0.0)$$

However, with this SFR we would expect S4 to have a U-band magnitude of the order $u(AB)=21$ from the continuum (assuming $\text{SFR} = L_{1500}/(1.6 \times 10^{40} \text{ erg s}^{-1} \text{ \AA}^{-1})$), which is not seen. Hence, star formation within S4 is very unlikely to be the source of the ionising photons.

4.2 The relation between DLAs and Lyman-break galaxies

At high redshift $z \sim 3$ the comoving mass density in neutral gas in the DLAs is similar to the mass density in stars today. In addition the global star formation rate in the DLAs at high redshift predicted from the rate of decline of the cosmic density of HI (Pei and Fall 1995) is in reasonable agreement with the measured global SFR in the Lyman break galaxies (Madau et al 1996), given the uncertainties in the two estimates. It is natural therefore to consider the connection between the two populations, DLAs and LBGs. To address this issue we will make the assumption that every LBG is surrounded by a DLA disk and ask whether it is then possible to reproduce the measured properties of the high- z DLA population.

A summary of the status of the search for LBGs was given by Dickinson (1998). Fig 9 in Dickinson (1998) provides the current best estimate of the luminosity function (LF) of galaxies at $z \approx 3$, for $q_0 = 0.5$. This estimate is quite uncertain for two reasons. Firstly it not yet clear how complete the LBG samples are, i.e. how many high-redshift galaxies fall outside their colour selection criteria. Secondly the faint-end slope of the LF, i.e. α in the Schechter parameterisation, is not well determined, relying as it does on the relatively small number of faint LBGs found in the Hubble Deep Field. Because of the small field of view of the HDF,

and the possibility of normalisation errors due to clustering, Dickinson (1998) rescaled the HDF numbers to tie smoothly on to the (well-determined) numbers at brighter magnitudes. For the present we will assume that the Schechter fit to the LF present by Dickinson (1998) is an adequate representation of the LF of LBGs.

Imagine now that every LBG lies at the centre of a DLA disk. To relate the LBG LF to observables of the DLA population we will suppose that the size of the DLA disk R_{gas} (i.e. the radius beyond which the column density falls below $2 \times 10^{20} \text{ cm}^{-2}$) is related to the galaxy luminosity by a power-law relation of Holmberg form $R_{gas}/R_{gas}^* = (L/L^*)^t$. The value of R_{gas}^* is fixed so as to reproduce the observed line density of DLAs dn/dz , i.e. the average number of DLAs per unit redshift along a line of sight to a quasar. For randomly inclined disks the relation between dn/dz and R_{gas}^* is (Wolfe et al. 1986, eqn nos 7, 8):

$$\frac{dn}{dz} = \frac{\pi c}{2 H} \Gamma(1 + 2t + \alpha) \phi^*(1+z)^{1/2} R_{gas}^{*2} \quad (q_0 = 0.5)$$

where Γ is the gamma function. For randomly inclined disks of radius R the average impact parameter is $\bar{b} = 0.524R$. Therefore

$$\bar{b}^* = 0.524 \sqrt{\frac{dn}{dz} \frac{2H}{\pi c \Gamma(1 + 2t + \alpha) \phi^*(1+z)^{1/2}}} \quad (q_0 = 0.5)$$

At $z = 3$ $dn/dz = 0.27$ (Wolfe et al., 1995). Together with the Holmberg relation this provides the expected average impact parameter as a function of apparent magnitude, at $z = 3$, and the expected apparent magnitude distribution of a sample of DLAs selected by gas cross section. Using Dickinson's LF these results are plotted in Fig. 6, for different values of the parameter t .

When using the predictions presented in Fig. 6 it is important to remember that both the normalization and faint end extrapolation of the LBG LF are at present poorly known. Also dn/dz for DLAs could be wrong by a significant factor, in case systematic effects due to lensing and/or dust obscuration by the DLAs are biasing the number counts. Nevertheless it is instructive to compare the predicted curves in Fig. 6 to the few detections currently available and in Fig. 6 we therefore also show the apparent magnitudes and impact parameters of the three confirmed DLA galaxies, and a single DLA galaxy candidate, from which continuum emission has been detected. Apparent magnitudes of the four objects have been transformed to $z = 3$ to enable comparison with the $z = 3$ LBG luminosity function.

We now compare properties of the known DLA galaxies against the predictions, to draw preliminary conclusions about the parameter t . It should be noted firstly that faint DLAs with small impact parameters would be very difficult to detect, so that the region $m_R > 26$ and $\bar{b} < 4h^{-1}$ is so far largely unexplored. On the other hand DLAs brighter than $m_R = 25$ at impact parameters $\bar{b} > 10h^{-1}$ kpc would be detectable from the ground. If $t = 1.0$ most of the LBG counterparts to DLAs would lie in this region, but the few actual detections are fainter and have small impact parameters. Therefore large values of t are not compatible with the observations.

For nearby spirals a value of $t \sim 0.4$ is measured (Wolfe et al., 1986). However, if the measured impact parameters of the few high-redshift DLAs detected are representative of

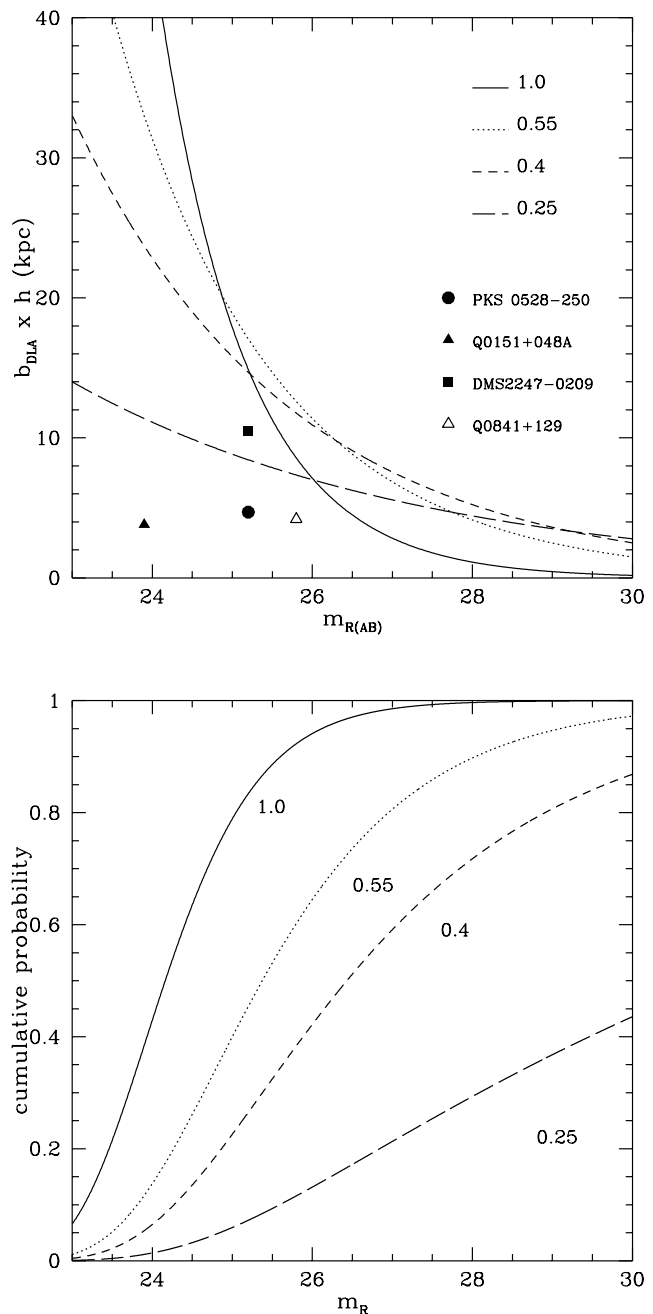


Figure 6. Predicted properties of the DLA population at $z = 3$ if DLAs are gaseous disks surrounding Lyman-break galaxies. *Upper:* the curves show predicted values of the mean impact parameter from the LBG to the line of sight to the quasar for different values of the Holmberg parameter t , as a function of apparent magnitude. The points are measured impact parameters for the three known DLA galaxies (and one likely candidate) for which the continuum magnitude of the galaxy has been measured. *Lower:* the curves show the predicted cumulative probability distribution for the apparent magnitudes of the LBG counterparts to the DLAs

the fraction of DLAs brighter than $m_R = 26$, a lower value of $t \sim 0.25$ is indicated. Referring now to the lower diagram of Fig. 6, this would have the consequence that $\approx 70\%$ of the LBG galaxy counterparts to DLAs at $z \approx 3$ are fainter than $m_R = 28$. This conclusion is in fact relatively insensitive to the (poorly-determined) faint-end slope of the LBG LF. For example if the actual value is either flatter or steeper than Dickinson's measured value, the curves in the upper part of Fig. 6 are different, and the value of t that passes through the data points is different. Nevertheless the corresponding curve in the lower plot for that value of t is quite similar to the lower curve shown.

In the nearby universe a sample of galaxies selected by gas cross section has a luminosity distribution peaked near L^* . The reason why this is probably not the case at high-redshift can be seen as follows. For a Schechter representation of the luminosity function the average luminosity of a sample of galaxies selected by gas cross section is $\bar{L} = L^* \Gamma(2 + \alpha + 2t) / \Gamma(1 + \alpha + 2t)$. Locally the canonical numbers for spirals are $\alpha = -1.25$ and $t = 0.4$ (Lanzetta et al 1991), yielding $\bar{L}(0) = 0.55L^*(0)$. At high redshift taking $\alpha = -1.38$ and $t = 0.25$ gives a much fainter average luminosity $\bar{L}(z) = 0.1L^*(z)$. This is a consequence of the fact that at high redshift the faint end slope of the luminosity distribution $\alpha + 2t$ is closer to the critical value -1.0 , which corresponds to zero average luminosity.

ACKNOWLEDGMENTS

Nordic Optical Telescope is operated on the island of La Palma jointly by Denmark, Finland, Iceland, Norway, and Sweden, in the Spanish Observatorio del Roque de los Muchachos of the Instituto de Astrofísica de Canarias.

J.U.F. wishes to thank B. Thomsen for many helpful discussions during preparation for the observing run and is grateful to E. Bertin for guidance in the use of SExtractor. J.U.F. and S.J.W. gratefully acknowledge support from the STScI and ESO visitors programmes, respectively. We thank our referee, Bruno Leibundgut, for many valuable comments which helped us clarify several points in the manuscript.

REFERENCES

- Bertin E, Arnouts S, 1996, A&AS, 117, 393B
 Bessell M. S., 1990, PASP, 281, 817
 Briggs F.H., Wolfe A.M., Liszt H.S., Davis M.M., Turner K.L., 1989, ApJ, 341, 650
 Colina L, Bohlin R.C., 1994, AJ, 108, 1931
 Dickinson M, 1998, preprint, astro-ph/980264
 Djorgovski S.G., Pahre M.A., Bechtold J., Elston R., 1996, Nature, 382, 234
 Djorgovski S.G., 1998, In: 'Structure and Evolution of the IGM from QSO Absorption Lines', ed. Petitjean P., Charlot S., (Editions Frontières), p.303
 Fukugita M., Shimasaku K., and Ichikawa T., 1995, PASP, 107, 945
 Fynbo J.U., Møller P., Warren S.J., 1998, In: 'Structure and Evolution of the IGM from QSO Absorption Lines', ed. Petitjean P., Charlot S., (Editions Frontières), p.408
 Ge J, Bechtold J., Walker C., Black J. H., 1997, ApJ 486, 727
 Giavalisco M., Steidel C. C., Macchetto F. D., 1996, ApJ, 470, 189
 Kennicutt R.C, 1983, ApJ, 272, 54
 Kulkarni V.P., Fall S.M., 1997, ApJL, 484, 17
 Landolt A.U., 1992, AJ, 104, 340
 Lanzetta K. M., Wolfe A. M., Turnshek D. A., Lu L., Mc Mahon R. G., Hazard C., 1991, ApJS, 77, 1
 Le Brun V., Bergeron J., Boissé P., Deharveng J.M., 1997, A&A, 321, 733
 Leibundgut, B., Robertson G., 1998, MNRAS, in press
 Lu L., Sargent W.L.W., Barlow T.A., Churchill C.W., Vogt S.S., 1996, ApJS, 107, 475
 Madau P., Ferguson H. C., Dickinson M. E., Giavalisco M., Steidel C. C., Fruchter A., 1996, MNRAS, 283, 1388
 Møller P., Warren S., 1993a, In *Observational Cosmology*, Chincharini, G., Iovino, A., Maccararo, T., Maccagni, D. (eds.), A. S. P. Conference series, **51**, 598
 Møller P., Warren S., 1993b, A&A, 270,43
 Møller P., Warren S., 1998, MNRAS, 299, 661
 Møller P., Warren S., Fynbo J., 1998, A&A, 330, 19
 Pei Y. C, Fall S. M., 1995, ApJ, 454, 69
 Pettini M., Hunstead R.W., King D.L., and Smith L.J., 1995, In: 'QSO Absorption Lines', ed. Meylan G., (Springer-Verlag), Berlin, p.55.
 Pettini M, King D.L., Smith L.J., Hunstead R.W., 1997, ApJ, 478, 536
 Robertson G., Leibundgut, B., 1998, In: 'Structure and Evolution of the IGM from QSO Absorption Lines', ed. Petitjean P., Charlot S., (Editions Frontières), p.271
 Steidel C.C., Pettini M., Dickinson M., Persson S.E., 1994, AJ 108, 2046
 Steidel C.C., Bowen D.V., Blades J.C., Dickenson M., 1995, ApJL, 440, L45
 Steidel C.C, Giavalisco M., Pettini M, Dickenson M., Adelberger K.L., 1996, ApJL, 462, L17
 Stetson P., 1994, "User's Manual for DAOPHOT II"
 Urbaniak J.J., Wolfe A.M., 1981, ApJ, 244, 406
 Warren S.J., Hewett P.C., Lewis G.F., Møller P., Iovino A., Shaver P.A., 1996, MNRAS, 278, 139
 Warren S., Møller P., 1996, A&A, 311,25
 Williams R.E, 1972, ApJ, 178, 105
 Wolfe A. M., Turnshek D. A., Smith H. E., Cohen R. D., 1986, ApJS, 61, 249
 Wolfe A.M., Lanzetta K.M., Foltz, C.B., Chaffee F.H., 1995, ApJ, 454, 698

This paper has been produced using the Royal Astronomical Society/Blackwell Science L^AT_EX style file.

This figure "field_col.gif" is available in "gif" format from:

<http://arxiv.org/ps/astro-ph/9812434v1>